

# On the ionizing continuum in active galactic nuclei: clues from ISO

M. Almudena Prieto<sup>1,2</sup> and Sueli M. Viegas<sup>3</sup>

<sup>1</sup>Instituto de Astrofísica de Canarias, Spain

<sup>2</sup>Max-Planck-Institut fuer extraterrestriche Physik, Garching, Germany

<sup>3</sup>Instituto Astronômico e Geofísico, São Paulo, Brazil

Received \_\_\_\_\_; accepted \_\_\_\_\_

## ABSTRACT

The ISO coronal line spectrum of the brightest Seyfert galaxies from the CfA sample is presented and modeled. ISO observations of [O IV] 25.9  $\mu$ , [Ne V] 14.3  $\mu$ , [Mg VIII] 3.02  $\mu$  and [Si IX] 2.58  $\mu$  lines are presented; their relationship with the soft part of the ionizing spectrum from 50 to 300 eV is investigated. Pure photoionization models reproduce the line ratios, setting ranges for the ionization parameter and the optical depth of the emitting clouds. On the basis of the available data alone it is not possible to distinguish between a power-law or a blackbody distribution as the intrinsic shape of the UV ionizing spectrum. However, for the brightest Seyferts analyzed, namely, NGC 1068, Circinus and NGC 4151, a black-body UV continuum is favored.

*Subject Headings:* galaxies: Seyfert - line: coronal - line: formation - infrared: galaxies

## 1. Introduction

The near-to-mid IR spectrum is extremely rich in emission lines from many different ionization stages including molecular, nebular and coronal lines from different species. Coronal lines are particularly suitable for deriving information about the UV to the soft X-ray region of the ionizing spectrum as they require photon energies above 50 eV. Pure starbursts, where [OIV] 25.9  $\mu$  is generally not present or very weak (Genzel et al. 1998; Lutz et al. 1998) do require photon energies below 50 eV. Thus, the study of coronal lines is unique for tracing the pure AGN power mechanism. Important coronal lines, particularly from Fe, are also present in the optical spectrum of some bright AGNs. However the larger extinction in the optical and the fact that reliable detection of these lines requires medium to high spectral resolution make the number of detections scarce. Alternatively, the IR region is less affected by extinction and proves to be ideal for detecting a wide range of coronal species. The availability of ISO allows us to make a systematic search for such coronal lines in Seyferts galaxies.

The CfA sample of Seyfert galaxies is the standard reference sample of active galactic nuclei in the nearby universe. For some of the brightest galaxies, a large wavelength range is covered, in particular, the UV, optical, infrared (IRAS) and radio. However, due to the large extinction affecting the Seyfert II type, very poor information is derived from the UV region and few reliable X-ray spectra are obtained for that class. An alternative to get clues on that part of the electromagnetic spectrum is via the study of the IR region. The sample of coronal lines studied in this work requires photon energies in the 50-300 eV range and therefore, their analysis can yield information about the extreme-UV-to-soft-excess continuum in AGN. With that aim in mind, the brightest Seyferts from the CfA sample were selected for observations with the SWS spectrometer on board ISO. Essentially, all those sources that were detected with IRAS at 12  $\mu$  were selected. Among those, there

are well known galaxies (e.g. NGC 4151, NGC 1068, NGC 3727) that were object of individual observations within the ISO guaranteed time programs and were not proposed for new observations with ISO. ISO SWS spectra of the coronal lines [O IV] 25.9  $\mu$ , [Ne V] 14.3  $\mu$ , [Mg VIII] 3.02  $\mu$  and [Si IX] 2.58  $\mu$  were collected for all of them. The sample is complemented with data from three brightest Seyfert galaxies — NGC 1068, Circinus (not CfA member) and NGC 4151— for which SWS spectra of those coronal lines are currently available in the literature. The final sample comprises seven Seyfert 2, four Seyfert 1 and one Seyfert 1.5 (Table 1).

## 2. The ISO coronal spectra of Seyfert galaxies

Our ISO observations were executed as follows. For each source, four individual SWS line spectra with resolution of about 200 km/s (SWS02 mode) and integration times per source between 1.5 and 2 hours were collected. Although the selected sample includes the brightest known Seyferts in the IR, i.e., all having been detected at 12 $\mu$  by IRAS, that did not prove to be sufficient when considering the sensitivity levels of the SWS02 mode. To keep within reasonable exposure times, only the coronal lines: [O IV] 25.9  $\mu$ , [Ne V] 14.3  $\mu$ , [Mg VIII] 3.02  $\mu$  and [Si IX] 2.58  $\mu$  were proposed for ISO observations. An additional serendipitous spectrum centered at about 4.6 $\mu$  was also obtained.

Data reduction of the SWS spectra was done at the ISO spectrometer data center at MPE using the Interactive Analysis IA package. Special routines built at MPE, aimed at improving spike removal, dark subtraction and flat fielding, were used. A minimum of five scans were collected per each ISO line spectrum to allow for deglitching.

As each SWS spectrum combines the information of 12 individual detectors, each covering different but overlapping regions of a given spectral window, the extraction of

the line spectrum requires a careful process. In particular, as redundant information from various detectors is summed up at the center of the line spectrum, the signal-to-noise ratio accumulated at the center of the spectral window is expected to be superior than that at the edges where there is less overlapping information. That translates into line spectra with higher signal-to-noise at the center but progressively degrading towards the edges. Nevertheless, the ISO line spectra were centered at the expected position of the corresponding line feature after correcting by the systemic velocity of the source. Thus, spectral features appearing at the expected position might be considered of large reliability.

For each galaxy, the ISO line spectra are shown in Figures 1a,b. The spectral resolution of the SWS mode is between 300 km/s for the long wavelength region and about 150 km/s for the short one. Typically, those are the binning sizes used to combine the individual scans to produce the final line spectrum.

The derived line fluxes and errors are given in Table 1. The errors reflect only the uncertainty in the continuum definition. Besides, the absolute flux scale of the SWS is accurate to about 25% (Schaeidt et al. 1996). Also, uncertainties in the lines position of up to 100 km/s may be expected due to pointing errors (Feuchtgruber et al. 1997).

In all cases, the strongest lines detected are [O IV] 25.9  $\mu$  and [Ne V] 14.3  $\mu$  lines whereas [Mg VIII] 3.02  $\mu$  and [Si IX] 2.58  $\mu$  are the most difficult to measure in both Seyfert types. Due to the low sensitivity level of the SWS in the short wavelength range, some of the apparent features in the ISO [Si IX] 2.58  $\mu$  and [Mg VIII] 3.02  $\mu$  spectra are uncertain. To keep on the safe side, all the reported fluxes for [Si IX] 2.58  $\mu$  and most for [MgVIII] 3.02  $\mu$  (Table 1) are given as upper limits or marked uncertain. These upper limits are either the integrated flux within the apparent feature or a 3 sigma limit (Table 1).

Mrk 817 is the only case with potential detection of both [Si IX] 2.58  $\mu$  and [MgVIII] 3.02  $\mu$ , as corresponding faint features at the expected position are seen in the ISO spectra

(Fig. 2). Additional possible detections of [Mg VIII] 3.02  $\mu$  are in Mrk 266 and Mrk 533. We marked those as uncertain since the apparent feature is shifted by  $\sim 200$  km/s in both galaxies. Besides, there are the relatively stronger detections reported for Circinus, NGC 1068 and NGC 4151 (Moorwood et al, 1996, Lutz et al, 1997 and Alexander et al. 1998, respectively), where [Si IX] 2.58  $\mu$  and [Mg VIII] 3.02  $\mu$  are clearly seen.

Regarding the [OIV]25.9  $\mu$  and [Ne V] 14.3  $\mu$  lines, they appear at the corresponding systemic velocity within the 100 km/s range for most of the sources. There are three exceptions where the [OIV]25.9  $\mu$  line is found substantially blueshifted. In NGC 5548, [OIV]25.9  $\mu$  is shifted by  $\sim -150$  km/s, which is in fair agreement with the shift of -134 km/s measured by Penston et al (1984) in the [FeX] 6374A line. In Mrk334 and NGC 5929, [OIV]25.9  $\mu$  shows shifted by about -300 km/s. An equivalent shift is not apparent in [Ne V] 14.3  $\mu$ . We note however that the general [OIV] and [NeV] line profiles in most of the Seyfert analyzed shows more complex than a single Gaussian profile. That prevents an accurate determination of the central line peak and the corresponding line shifts, particularly if the S/N is not sufficiently high.

[FeII] 25.98  $\mu$  line was also found in some of the galaxies in the sample. Due to its proximity to [OIV] 25.9  $\mu$ , that line can also be seen in the ISO [OIV]25.9  $\mu$  spectrum. Detections of the FeII line are seen in Mrk 266, NGC 5929, Mrk 334 and Mrk 817 (Fig. 1ab). Due to the poor spatial resolution of ISO – SWS aperture sizes range from 14x20 arcsec at short wavelengths to 20x33 arcsec at long wavelengths – the integrated [FeII]25.98  $\mu$  emission may mostly comes from the star forming regions in the disc of these galaxies. As the present analysis focuses on the central AGN source, that line is not considered for the modeling purposes.

### 3. Modeling the IR lines

The presence of high ionization lines in the far infrared spectrum of Seyfert 1 and 2 is probably the signature of high energy photons produced in the central source, providing highly ionized gas. From this point of view, the analysis of the 2.5 - 45  $\mu$  ISO spectrum of Circinus (Moorwood et al. 1996) indicated that the ionizing radiation spectrum should have an UV bump, represented by a  $2 \times 10^5$  K blackbody radiation, added to a X-ray power-law, with spectral index  $\alpha_X = -0.5$ . The IR lines are roughly reproduced, the coronal lines being fitted within a factor of 2. A further detailed analysis of the *multiwavelength emission-line and continuum spectra* (Contini, Prieto & Viegas 1998a), indicates a more complex scenario for Circinus central region. That basically requires a weighted contribution of clouds with different densities and optical depth, some of them showing the effect of high-velocity shocks.

The present analysis is restricted to the set of coronal lines discussed in section 2, which were systematically observed by ISO for all the galaxies in the sample. They are used to test the ionizing continuum shape in these galaxies on the basis of photoionization models only. More elaborated analysis based on a multiwavelength analysis approach – as those done for the Seyferts prototype Circinus and NGC 5252 (Contini, Prieto & Viegas 1998a,b) – are out of the scope of this paper.

The behavior of the observed line ratios [Ne V]/[O IV], [Mg VIII]/[O IV] and [Si IX]/[O IV] versus the ionization potential (IP) of  $\text{Ne}^{3+}$ ,  $\text{Mg}^{6+}$  and  $\text{Si}^{7+}$  is shown in Figure 2ab. The brightest galaxies, for which clear detections of [Si IX] 2.58  $\mu$  and [Mg VIII] 3.02  $\mu$  exist, show a common trend of decreasing line ratios with the IP. The other galaxies of the sample shows also a clear decrease toward [MgVIII]/[OIV]. However, if we extend the plot in order to include [SiIX]/[OIV], the overall behavior is equally consistent with a decreasing trend or a valley shape – [SiIX]/[OIV] larger than [MgVIII]/[OIV] –. If the detection of

[SiIX]  $2.58 \mu$  in Mrk 817 is confirmed, a valley shape is found.

Regarding [Ne V]/[O IV] and [MgVIII]/[O IV] line ratios, the Seyfert 2 sample present values within the range measured for Circinus and NGC 1068 (figure 2). A clear exception is NGC 5929, but this galaxy presents a weak ISO coronal line spectrum. In the case of the Seyfert 1 sample, the [Ne V]/[O IV] and [Mg VIII]/[O IV] values are in all cases larger than in NGC 4151. Although most of the [Mg VIII] values are upper limits, note however that the [NeV] and [OIV] lines are well determined for this sample.

With the above caveats in mind, the present modeling investigates the relationship between the coronal line ratios and the ionizing radiation spectrum required to form the corresponding ions. The photoionization simulations are obtained with the photoionization code Aangaba (Gruenwald & Viegas 1992) which has been compared to similar codes (Ferland et al. 1995). The basic assumptions considered in the current modeling are plan-parallel symmetry, solar abundances, and a composite ionizing spectra (blackbody plus an X-ray power law, or two power-laws). For the X-ray component, we adopt the canonical power-law index for AGN  $\alpha_X = -0.7$ . Firstly, we discuss the results for two types of UV continuum, namely, a  $2. \times 10^5$  K blackbody and a power-law with power index  $\alpha_{UV} = -2.0$ . In both cases, the UV spectrum reaches the X-ray regime at  $E \simeq 100$  eV. We anticipate that variations in the black-body temperature or the UV spectral index do not introduce significant differences in the model results; however, these are more sensitive to changes in the  $E_c$  value.

The critical density of the coronal emission lines is high, so the results are practically independent of the gas density as long as  $ne \leq 10^5 \text{ cm}^{-3}$ . Thus, the two parameters that are left free are *the ionization parameter*  $U$  (ratio of the number density of ionizing photons and the gas density), *and the cloud optical depth*, characterized by the optical depth at the Lyman limit,  $\tau_{ly}$ .



The line ratios versus IP are shown in Figures 3a (UV blackbody) and 3b (UV power law). The top panel shows the results for a given U and varying  $\tau_{ly}$ , and the bottom panel the theoretical ratios for an optically thick cloud ( $\tau_{ly} \geq 30$ ) at different U values. Both set of models produce [NeV]/[OIV] and [Mg VIII]/[O IV] values within the limits that are observed in the present sample. A first result illustrated by the figures is that for both set of UV ionizing continuum, an overall “valley shape” is generally produced.

Blackbody models with low  $\tau_{ly}$  ( $\leq 2$ ) show a different behavior, namely, the line ratios increasing with the ionization potential (upper part in fig 3a). This is because the optically thin models tend to penalize the lower ionization lines, favoring the high ionization zone. The ratios are relative to [O IV]. This line originates in the O<sup>3+</sup> region which decreases with  $\tau_{ly}$  faster than Mg<sup>6+</sup> and Si<sup>7+</sup> zones; thus, [Mg VIII]/[O IV] and [Si IX]/[O IV] tend to become higher as  $\tau_{ly}$  decreases.

Conversely, blackbody models with low U value tend to smear out the valley shape by producing slightly lower [Si IX]/[O IV] than [Mg VIII]/[O IV] (fig 3a). A similar effect occurs as well in the case of the UV power law model, but in this case the effect is much more dramatic as the [Si IX] and [Mg VIII] lines tend to vanish (lower part in fig 3b).

If an UV power index  $\alpha_{UV} = -1.5$  is adopted, the results are very similar, all the models showing a valley shape even in the case of low  $\tau_{ly}$  values. In this case the O<sup>3+</sup> zone is closer to the cloud edge facing the central radiation source and thus, less affected by matter-bounded conditions. Regarding the UV black-body, variations in the temperature within a few  $10^5$  K do not modify the general trend shown in Fig 3a.

Summarizing, within the set of model parameters considered, both UV models (blackbody and power-law) predict similar results, namely, a valley shape relationship between the coronal line ratios and the ionization potential required to produce the corresponding ions. This model result can easily account for the case of Mrk 817 if the

[SiIX]2.58  $\mu$  and [Mg VIII] 3.02  $\mu$  lines turn to be reliable detections; yet, it clearly departs from the most solid trend seen in the brightest Seyferts, NGC 1068, Circinus and NGC 4151. In these cases, the observed line ratios show a straight decreasing trend vs the ionization potential.

### 3.1. Diagnostic diagrams

The four observed coronal lines allows us to construct two diagnostic diagrams. These are discussed on the basis of the model predictions for the two types of UV continuum considered.

Focusing first on the observed line ratios (plotted in Figures 4), a general trend is suggested in both diagrams, in the sense that both [SiIX]2.58  $\mu$  and [Mg VIII] 3.02  $\mu$  lines relative to [OIV] tend to increase with increasing [NeV]/[OIV]. This trend is surprising if considered that most of the [SiIX]2.58  $\mu$  and [Mg VIII] 3.02  $\mu$  measurements are taken as upper limits.

If considered the UV black-body models, the observed trend can be reproduced for  $U \leq U_c = 0.1$ , and optically thick clouds,  $\tau_{ly} \gg 1$  (Fig 5a,b). The upper limits for [MgVIII] and [SiIX] will just move the points down in the diagram suggesting lower U values. Indeed, this is the case for the brightest Seyferts which require U values below 0.01 (discussed in next section).

In the case of UV power law models (Fig. 6a,b), the predicted line ratios always increase with U, for  $U \leq U_c = 1$  (this being the main difference with the black-body models). Besides, for  $\tau_{ly} \geq 1$ , the theoretical ratios predicted by the power law models become very similar. The comparison with the observational data indicates similar range of U values as in the blackbody case but the emitting clouds are closer to the optically thin

case, with values in the range  $0.2 \leq \tau_{ly} \leq 1.0$  for most of the objects.

### 3.2. The brightest Seyferts

In an attempt to account for the line ratio trend shown in Fig.2 by NGC 1068, Circinus and NGC 4151, the UV black-body models are explored in more detail in this section. Models with an UV power law were also built but the results were less encouraging.

Varying the black-body temperature within a few of  $10^5$  K, the best representation of the observed trend is obtained for  $T \sim 2 \times 10^5$  K and  $\alpha_X = -0.7$ . Furthermore, the ionization parameter should remain low ( $U \simeq 0.03$ ) and the optical depth be larger than unity. Larger  $U$  or lower  $\tau_{ly}$  tend to generate the “valley shape” discussed in section 3. In this case, the zone producing the [O IV] line is not so wide, the [O IV] is weaker and the line ratios become higher.

In all the models discussed in former sections, the adopted value for the energy break between the UV black-body and the X-ray power-law was set to  $E_c = 100$  eV. However, we may expect that slight variations in  $E_c$  significantly affect the line ratios, particularly those involving SiIX and MgVII, as 100 eV is within the range of IP values required produce those ions.

The final results are as follows. The best match to the data is found for  $E_c = 120$  eV,  $U = 0.01$  and optical depths about 1.5 or larger. Models with optical depth between 1.5 and 30 produce very similar results provided that the ionization parameter remains low. The results are plotted in Fig. 7: only two set of models are shown. The first set of models corresponds to  $U = 0.01$  (two models are plotted for  $\tau = 1.5$  and 30 respectively). The second set of models corresponds to lower  $U = 0.005$  (plotted for  $\tau = 1.5$  and 30). In all cases,  $E_c = 120$  eV. For larger  $E_c$ , the predicted  $[\text{NeV}]/[\text{OIV}]$  gets too strong compared

with the data (see also Fig 5ab). In fact, because the UV black-body continuum is steeply decreasing at these energies, larger values of  $E_c$  would favor the production of  $O^{+3}$  and  $Ne^{+4}$  instead of increasing the higher ionized ions: i.e.,  $[NeV]/[OIV]$  tends to increase faster relative to  $[Mg\ VIII]/[OIV]$  and  $[Si\ IX]/[OIV]$ .

The models just described provide a rough approximation of the observed trend. No attempt was made to fit the individual line ratios because we expect that various clouds at different conditions should contribute to the observed spectrum. In particular, the higher ionization lines ( $[Mg\ VIII]$  and  $[Si\ IX]$ ) may be produced in clouds different from those producing the lower ionization ones ( $[O\ IV]$  and  $[Ne\ V]$ ). In addition, changes in the relative abundances (current modeling is for solar abundance) can play a major role in fitting individual line ratios.

Recently, Binette (1998) discussed models for the coronal lines of Circinus and NGC 1068, assuming the ionizing continuum represented by two power laws, with power index equal to 1.3 in the infrared-UV range and 0.7 in the X-ray range, and joining at  $E_c = 2000$  eV. Such a high  $E_c$  value makes the ionization structure of the gas to be mainly determined by the UV continuum. His model includes radiative acceleration of the coronal gas, which results in gas compression by factors of 1.6 to 2.6. From the fraction of unabsorbed ionized photons listed in his paper, we deduce that the optical depth of the cloud is also greater than unity. However, for both galaxies the ionization parameter is greater than 0.1. The difference with our models comes from the shape of the UV continuum which in his case is flatter than that used in our models. This flatter spectrum coupled to the increase of the gas density due to compression, makes the lower ionized zone (where  $[O\ IV]$ ,  $[Ne\ V]$ ,  $[Si\ VI]$ ,  $[Fe\ VII]$  originate ) narrower than the higher ionized zone. Thus the trend of the line ratios decreasing with the ionization potential discussed above cannot be reproduced. For this, lower values of  $U$  ( $\simeq 0.01$ ) must be considered. But, in this case the Fe coronal lines

relative to [Si IX] (as used by Binette) become too strong.

Binette’s models and ours clearly indicate that a good fit to the coronal lines can only be achieved if the contribution from several clouds at different physical conditions are taken into account.

#### 4. Conclusions

The ISO spectra of the coronal lines [O IV] 25.9  $\mu$ , [Ne V] 14.3  $\mu$ , [Mg VIII] 3.02  $\mu$  and [Si IX] 2.58  $\mu$  for a sample of bright Seyfert type 2 and 1 galaxies are presented. To produce the ionization states that give rise to those fine-structure lines, energies in the 50 - 300 eV range are required. Accordingly, by studying those lines, clues on that soft part of the ionization continuum can be derived.

The emission lines [O IV] 25.9  $\mu$  and [Ne V] 14.3  $\mu$  are found to be common strong features in the Seyfert spectra regardless of their type. On the other hand, [Mg VIII] 3.02  $\mu$  and [Si IX] 2.58  $\mu$  are much weaker and for most cases, just an upper limit is provided.

The ratio of these coronal lines relative to [O IV] 25.9  $\mu$  are compared to model predictions derived under pure photoionization conditions. Two type of UV ionization continuum, namely, a power-law and a hot blackbody, are used. Within a reasonable range of values for the ionization parameter U, and the optical depth of the clods,  $\tau_{ly}$ , both type of models appear indistinguishable on the basis of these data alone.

However, some constrains on the ionization parameter and the optical depth of the emitting clouds can be derived. Independent on the UV continuum model selected, values of the ionization parameter below 0.1 are required. This is mostly to account for the systematic low [SiIX]/[OIV] ratios indicated by the data. The optical depth of the emitting clouds,  $\tau_{ly}$ , is more UV-continuum model dependent but in general values about 1 or

larger are indicated for most of the sources. Specifically, the range of  $\tau_{ly}$  indicated by the data varies from optically thin to optically thick clouds in the case of an UV power law distribution whereas optically thick clouds are mostly indicated in the case of an UV blackbody.

Focusing on the brightest Seyfert in the sample, Circinus, NGC 1068 and NGC 4151, for which accurate measurement of the above coronal lines is available, a more clear pattern arises. They all show a decreasing trend of the ratio of the coronal lines relative to [O IV]  $25.9 \mu$  as a function of the ionization potential (required to produce the emitting ion). Our best approximation to that pattern is obtained by assuming an UV black-body with a cutoff energy in the 100 - 120 eV range. Furthermore, U values below 0.01 and  $\tau_{ly}$  larger than 1 are required. In fact, low U values couple to large values of  $\tau_{ly}$  favor the presence of lower ionization ions such as  $O^{+3}$  compared to  $Si^{+8}$ , consequently decreasing the [SiIX]/[OIV] ratio. In addition, if the cloud is optically thick, the volume emitting [O IV] is larger, and the [SiIX]/[OIV] ratio is still lower as seen in NGC 4151.

Other facts however are expected to contribute as well to that pattern. First the all, these line ratios depend on the abundance ratios like Ne/O, Mg/O and Si/O whereas simply solar ratios are assumed in our models. Second, a reliable determination of the ionizing radiation spectrum could only be obtained if a mixing of clouds with different U and  $\tau_{ly}$  is chosen to fit several emission-line intensities in a more complete multiwavelength study.

**Acknowledgments:** It is a pleasure to thank Dietmar Kunze and Eckhard Sturm from the ISO Spectrometer Data Center at MPE for their constant support in the processing of the SWS data. The referee, Dieter Lutz, is acknowledged for his critical review. MAP is thankful to Fapesp for allowing her visit to IAGUSP, Brazil. This work is partially supported by FAPESP, CNPq and PRONEX/Finep, Brazil.

- Binette, L., 1998, MNRAS 294, L47
- Binette, L., Wilson, A, Raga, A. & Storchi-Bergmann, T. 1997 A&A  
327,909
- Contini, M., Prieto, M. A., & Viegas, S. M. 1998a, ApJ 492, 511
- Contini, M., Prieto, M. A., & Viegas, S. M. 1998b, ApJ 505, 621
- Ferland et al. 1995, in The Analysis of Emission Lines, STScI Symp.  
Ser. 8, ed. R. E. Williams & M. Livio (Cambridge: Cambridge Univ.  
Press), 143
- Feuchtgruber et al 1997, ApJ 487, 962
- Genzel, R. et al, 1998, ApJ 498, 579
- Gruenwald, R. & Viegas, S. M. 1992, ApJS 78, 153
- Lutz, D., Sturm, E., Genzel, R. Moorwood, A. & Sternberg, A. 1997,  
Ap&SS 248, 217
- Lutz, D., Kunze, D., Spoon H., Thornley, M. 1998, A&A 333, L75
- Moorwood, A.F.M., Lutz, D., Oliva, E., Marconi, A. Netzer, H.,  
Genzel, R., Sturm, E., & de Graauw, Th. 1996, A&A 315, L109
- Penston et al, 1984, MNRAS 208, 347
- Schaeidt, S. G. et al., 1996, A&A 315, L55
- Sturm, E., Alexander, T., Lutz, D., T., Sternberg, A., Netzer, H. &  
Genzel, R., 1999, ApJ 512, 197

Table 1: ISO coronal line fluxes for Seyfert galaxies

Name	Syf	V	[SiIX]	[MgVIII]	[NeV]	[OIV]
	Type	Km/s	$2.59\mu$	$3.03\mu$	$14.3\mu$	$25.9\mu$
N5548	1	5152	$<4.9\text{e-}21$	$<2.\text{e-}21$	$8.9\text{e-}21 \pm 30$	$7.5\text{e-}21 \pm 10$
N5929	2	2490	$< 4.9\text{e-}21$	$< 1.1\text{e-}21$	$<3.5\text{e-}21 \pm 50$	$2.1\text{e-}21 \pm 40$
Mrk817	1	9436	$3.1\text{e-}21 ?$	$1.1\text{e-}21 ?$	$6.9\text{E-}21 \pm 30$	$3.12\text{e-}21 \pm 13$
Mrk335	1	7688	$< 1.\text{e-}21$	$< 1.\text{e-}21$	$< 1.2\text{e-}20$	$1.9\text{e-}20 \pm 30$
Mrk266	2	8360	$< 5.8\text{e-}21$	$1.8\text{e-}21 ?$	$5.\text{e-}21 \pm 30$	$2.1\text{e-}20$
Mrk533	2	8670	$< 7.2\text{e-}21$	$1.8\text{e-}21 ?$	$1.1\text{e-}20 \pm 20$	$3.2\text{e-}20$
Mrk334	2	6582	$< 2.9\text{e-}21$	$< 1.3\text{e-}21$	$2.7\text{e-}21 \pm 30$	$4.3\text{e-}21$
N1144	2	8648	$< 4.9\text{e-}21$	$< 1.4\text{e-}21$	$7\text{e-}21 \pm 30$	$8\text{e-}21$
N5033	1	876	$< 3.57\text{e-}21$	$< 1\text{e-}21$	$6.1\text{e-}21 \pm 20$	$1.2\text{e-}20$
CIRCI	2	436	$1.8\text{e-}20$	$6.5\text{e-}20$	$44\text{e-}20$	$72\text{e-}20$
N1068	2	1140	$4.1\text{e-}20$	$14\text{e-}20$	$97\text{e-}20$	$160\text{e-}20$
N4151	1.5	980	$2.3\text{e-}21 \pm 20$	$6.2\text{e-}21$	$55\text{e-}21$	$20\text{e-}20$

Fluxes are in  $W \text{ cm}^{-2}$ . Upper limits are derived from the most promising feature in the spectra; otherways a 3 sigma limit is given. Errors in the flux (indicated in percent) only reflect the uncertainty in defining the continuum level; when no indicated, the errors are within 10%. Uncertain identifications are marked with a question mark. Data from Circinus are taken form Moorwood et al (1996); NGC 1068 from Fig. 2 in Lutz et al (1997); NGC 4151 from Sturm et al. (1999). Redshift and Seyfert type are taken from NED.



## Figure Captions

Figure 1a,b - ISO spectra for the sample of observed Seyfert 1 (a) and 2 (b) galaxies. Each row corresponds to a given galaxy identified in the first panel. Y-axis represents absolute flux in Jy; X-axis is the redshifted spectrum measured with respect to the position of the expected line in  $\mu$ . The given range is equivalent to about  $\pm 1000$  km/s about the central position. First panel in each row corresponds to [MgVIII] 3.02  $\mu$ ; second to [SiIX] 2.58  $\mu$ , third to [NeV] 14.3  $\mu$ ; fourth shows [OIV] 25.9  $\mu$  and [FeII] 25.98  $\mu$  (in this case, the x-axis is measured with respect to the position of the [OIV] line, the total range is about 3000 km/s).

Figure 2a,b - Coronal emission-line intensities relative to [O IV] 25.9  $\mu$  as a function of the ionization energy required to produce the emitting ion for, (a) Seyfert 1 galaxies: NGC 5548(solid triangle), Mrk 817(solid square), Mrk 335(solid circle), NGC 5033(star), NGC 4151(circle), and (b) Seyfert 2 galaxies: NGC 5929(solid triangle), Mrk 266(solid square), Mrk 533 (solid circle), Mrk 334(star), NGC 1144(circle), Circinus(empty square), NGC 1068 (empty triangle) Data for Circinus, NGC 1068 and NGC 4151 are joined by lines.

Figure 3a - Coronal emission-line intensities, relative to [O IV] 25.9  $\mu$ , from photoionization models with a blackbody UV ionizing radiation. The top panel show the results for the models with  $U = 0.2$  and  $\tau_{ly} = 0.2, 1., 2., 3., 5.$  and  $30$  (solid, dotted, dashed, long-dashed, dot-dashed and solid, respectively). A model corresponding to  $U = 0.006$  and  $\tau_{ly} = 30$  is also showed (bottom dashed line). The bottom panel show optically thick models with different values of the ionizing parameter  $U = 0.4$  (higher solid line) to  $0.006$  (bottom dashed line).

Figure 3b - Coronal emission-line intensities, relative to [O IV] 25.9  $\mu$ , from

photoionization models with a power-law UV ionizing radiation. The top panel show the results for the models with  $U = 0.2$  and  $\tau_{ly} = 0.2, 1., 2., 5.$  and  $30$  (solid, dot-dashed, dotted, dashed, and solid, respectively). A model corresponding to  $U = 0.006$  and  $\tau_{ly} = 30$  is also showed (lower dashed line). The bottom panel show optically thick models with different values of the ionizing parameter  $U = 0.4$  (higher solid line) to  $0.006$  (lower solid line).

Figure 4 - Diagnostic diagrams for the IR coronal lines: data The triangles correspond to Syf 1 and solid circles to Syf 2. Those galaxies with uncertain detection of [MgVIII] (Mrk 266 and Mrk 533) and [SiIX] (Mrk 817) are identified. Also the brightest Seyfert NGC 1068, NGC 4151 and Circinus are marked.

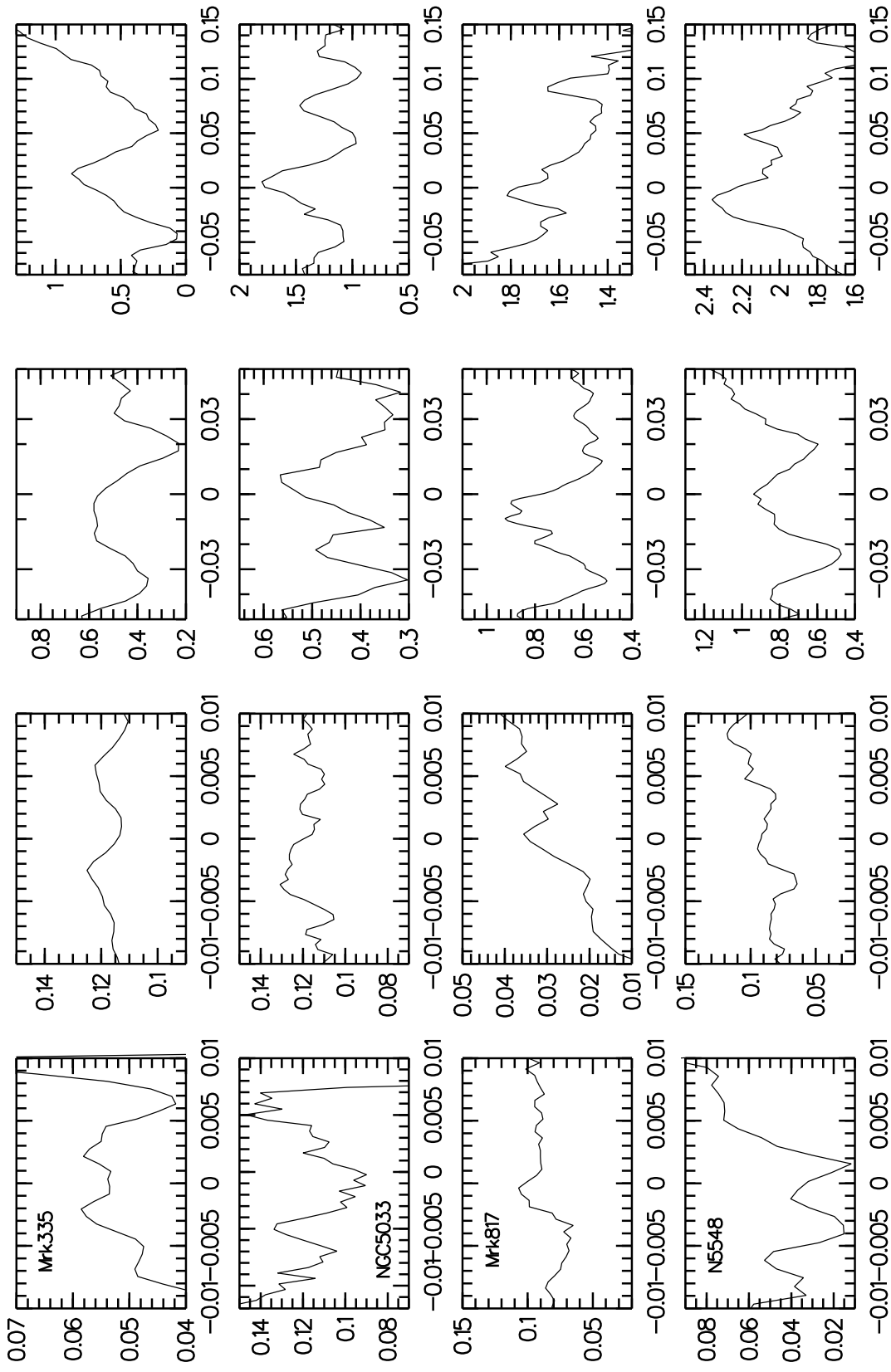
Figure 5a,b - Diagnostic diagrams for the IR coronal lines: data plus models. Theoretical results correspond to models with UV blackbody radiation and  $E_c=100$  eV. Each curve correspond to models with different values of  $U$  and a given  $\tau_{ly} = 0.2, 1., 5.$  and  $30$  (solid, dot-dashed, dashed, and solid, respectively). The observed data are overimposed: the triangles correspond to Sy 1 and solid circles to Sy 2. The thick line correspond to a model with cut-off energy  $E_c= 120$  eV and  $\tau_{ly} = 1.5$ .

Figure 6a,b - Diagnostic diagrams for the IR coronal lines. Theoretical results correspond to models with UV power-law radiation. Each curve correspond to models with different values of  $U$  and a given  $\tau_{ly} = 0.2, 0.3, 1.$  and  $30$  (solid, short-long dash, dot-dashed, and solid, respectively). The observed data are overimposed: the triangles correspond to Sy 1 and solid circles to Sy 2 results.

Figure 7 - Coronal emission-line intensities relative to [O IV]  $25.9 \mu$  as a function of the the ionization energy required to produce the emitting ion for NGC 1068 (square), Circinus (triangle) and NGC 4151 (circle). Two set of models for an UV black-body radiation and cut-off energy  $E_c= 120$  eV are displayed: dot lines refer to  $U=0.01$  and  $\tau_{ly}= 1.5$  and  $30$ ;

dash lines refer to  $U=0.005$  and same  $\tau_{ly}$  as before.

ISO-SWS/ Seyfert 1



ISO-SWS/ Seyfert 2

